ACS Energy LETTERS

http://pubs.acs.org/journal/aelccp

Early Stage Li Plating by Liquid Phase and Cryogenic Transmission Electron Microscopy

Hayoung Park,[▽] Yonggoon Jeon,[▽] Woo Jun Chung, Yuna Bae, Jihoon Kim, Hayeon Baek, and Jungwon Park*

Cite This: *ACS Energy Lett.* 2023, 8, 715−721

Read Online

ACCESS | Metrics & More | Article Recommendations | Supporting Information

ABSTRACT: **Li metal anodes are among the most promising options for next-generation batteries, exhibiting the highest theoretical capacity. However, irregular Li electrodeposition, which raises safety concerns, is a major obstacle in practical applications. Therefore, a fundamental understanding of the beginning phases of Li plating, such as nucleation and early growth, which have a decisive influence on the dendritic growth of Li, is essential. In this study, we investigated the early stage of Li plating at the single-particle level and its correlation with the solid-electrolyte interphase (SEI) using *in situ* liquid phase transmission electron microscopy (TEM) and cryogenic TEM. We observed contrasting nucleation dynamics and particle growth patterns in two electrolytes (1 M $LiPF_6$ in ethylene carbonate/diethyl carbonate and 1 M LiTFSI in 1,3-dioxolane/dimethoxy ethane), which originate from different chemical and physical properties of the SEIs. Based on our findings, we propose a mechanism of nucleation and initial growth of Li dictated by the SEI.**

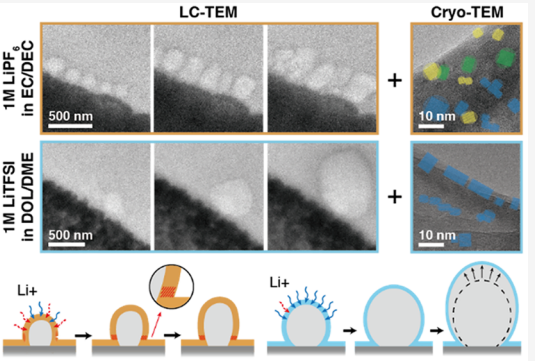

Lithium is the most promising alternative anode material for conventional graphite anodes due to its extremely high theoretical capacity (3,860 mAh/g) and low negative reduction potential (−3.04 V vs standard hydrogen electrode).[1−3] However, the uncontrolled morphological evolution of Li, such as the formation of whiskers, globules, and moss, is a major hurdle for the commercialization of Li metal batteries (LMBs).[4−6] When Li grows into dendrites, it leads to short-circuit and, more seriously, heat generation and thermal runaway, threatening its safety.[7] The dynamics of Li plating is primarily regulated by a solid-electrolyte interphase (SEI). SEI is unavoidably formed on the Li surface owing to the high reactivity of Li with organic electrolytes.[8−10] Low ionic conductivity, nonuniform thickness, or structural inhomogeneity of the SEI is known to induce dendritic growth of Li.[11,12] Therefore, chemical and physical characteristics of the SEI are key components that determine the kinetic pathway of Li growth.

As electrochemical Li growth is a kinetically driven process, the irregular nature of Li evolution is likely to initiate from the beginning phase of Li electrodeposition. After the formation of the SEI on the electrode in the early stages of Li deposition, it can be predicted that the SEI regulates the transport of Li-ion species and electrochemical reduction of Li at the interface of the electrode and SEI.[13,14] However, understanding the properties of the SEI and its role in the electrodeposition of Li is not trivial because the SEI is a product of the complex chemical and electrochemical reactions of the electrolyte. A common electrolyte is prepared by mixing several components, including solvents, salts, and various additives. In addition, there is a wide range of choices for each chemical category and their combinations.[15−17] Due to this complexity, the SEI inherently possesses heterogeneity with respect to the compositional domains and their distribution within the SEI when it is formed on the surface of the electrode.[18,19] Furthermore, such heterogeneous SEI structures vary depending on the combination of chemicals used for preparing the electrolyte mixture.[17,20−23]

Recently, many studies have attempted to investigate the nucleation stage of Li using post-mortem analysis, modeling, and simulation.[12,13,24,25] For example, in a post-mortem analysis using scanning electron microscopy, it was found that the nucleation density and nuclei size, based on classical nucleation theory, are determined by the current density.[13,24] Other studies, based on modeling and simulation, have shown that the

Received: October 22, 2022
Accepted: December 23, 2022

https://doi.org/10.1021/acsenergylett.2c02387
ACS Energy Lett. 2023, 8, 715−721

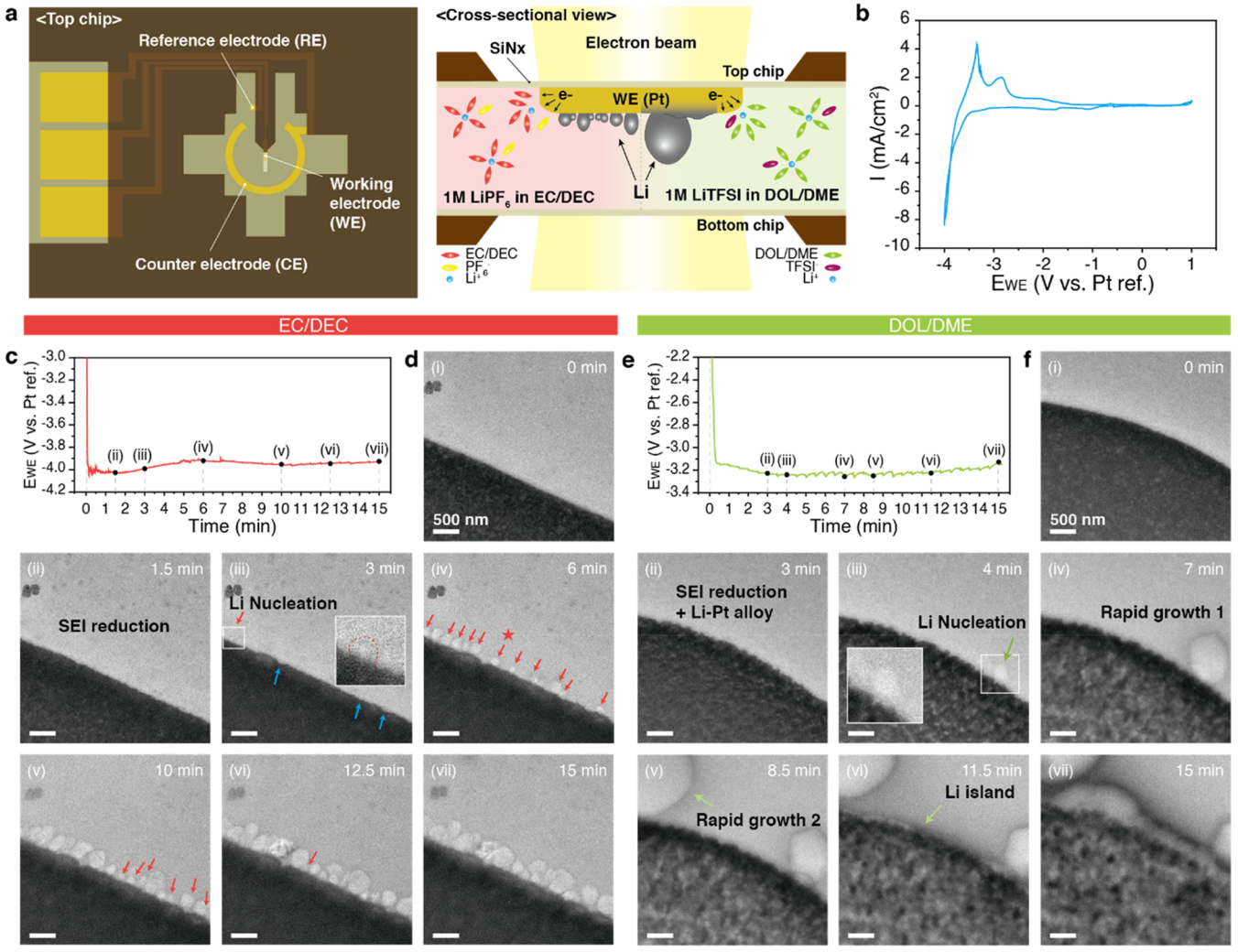

Figure 1. (a) Schematic illustration of *in situ* liquid cell microchip and Li formation in two electrolytes within a microcell. (b) Cyclic voltammetry (scan rate 20 mV/s) in 1 M $LiPF_6$ in ethylene carbonate/diethyl carbonate (EC/DEC) electrolyte. (c) The voltage profile of galvanostatic plating with 0.5 mA/cm^2 and (d) the time-series transmission electron microscopy (TEM) snapshots during Li plating in EC/DEC. (e) The voltage profile of galvanostatic plating with 0.5 mA/cm^2 and (f) the time-series TEM snapshots during Li plating in 1 M LiTFSI in 1,3-dioxolane/dimethoxy ethane (DOL/DME). (i) corresponds to a pristine state before plating and (ii–vii) correspond to the six points in the voltage profile. The insets in panels d and f are magnified images of Li nucleation. The red and green arrows in panels d and f, respectively, indicate newly formed nuclei at the time point, and the blue arrows in panel d indicate the defects on the electrode.

current density and properties of the SEI, such as mechanical strength and ionic conductivity, affect the heterogeneity of Li nucleation.[12,25] However, understanding the underlying mechanism for Li electrodeposition still requires a clear picture of the complex SEI structures and direct interpolation between these SEI structures and their roles in Li nucleation kinetics. If liquid phase transmission electron microscopy (TEM) and cryogenic-TEM (cryo-TEM) are combined and successfully applied to study Li growth, it will enable direct visualization of Li growth in a realistic liquid electrolyte and elucidation of the nanoscale structures of sensitive Li and SEI, along with their representations in Li growth.[26−29]

In this study, we investigated single-particle nucleation events, their subsequent early stage growth, and the associated SEI structures occurring in Li plating by *in situ* liquid phase TEM combined with cryo-TEM. Our study revealed that the chemical composition, uniformity, and mechanical properties of SEI collectively determine the dynamics of nucleation and initial growth in different electrolyte systems. In 1 M $LiPF_6$ in ethylene carbonate/diethyl carbonate (EC/DEC, 1:1 vol %), Li grows slowly with high nucleation density, which is attributed to the low Li^+ diffusivity and poor stability of the SEI. In contrast, in 1 M LiTFSI in 1,3-dioxolane/dimethoxy ethane (DOL/DME, 1:1 vol %), Li grows rapidly, often in a stepwise manner, with sparse nucleation events originating from the high Li^+ conductivity and flexibility of the SEI. This study provides a clear picture of the initial Li electrodeposition process, which is heavily affected by the SEI in LMB systems.

We explored the initial stage of Li plating in EC/DEC and DOL/DME, representative systems of carbonate and ether-based electrolytes, respectively, by *in situ* biasing liquid phase TEM. The liquid-phase microcell for Li growth was established with a top chip on which the Pt electrodes are patterned and a bottom chip, as shown in the schematic in Figure 1a (Experimental Methods). A cyclic voltammogram obtained from the microcell showed a large cathodic current for Li reduction and two anodic peaks for delithiation, which was consistent with that of a LilPt half-cell, revealing the reliability of

https://doi.org/10.1021/acsenergylett.2c02387
ACS Energy Lett. 2023, 8, 715−721

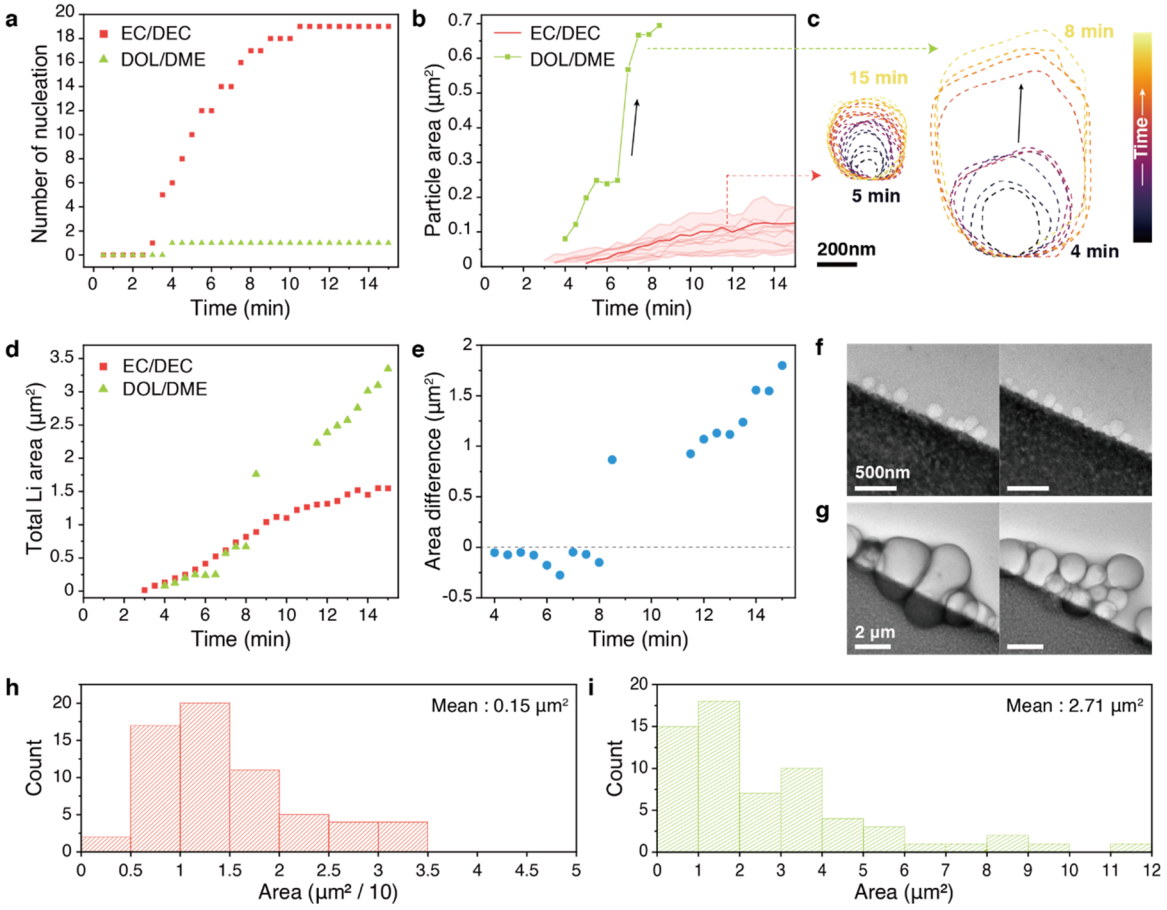

Figure 2. (a) Number of nucleation sites in both systems. (b) Changes in individual Li particle area. The particles are plotted until they exit the frame. All profiles are compared between EC/DEC and DOL/DME within a uniform field of view. (c) The contour trajectories during plating in EC/DEC (left, corresponding to the red bold line in panel b and the particle marked as red star in Figure 1d) and DOL/DME (right). (d) The profile for the total reacted area of all lithium particles. (e) The change in difference between total Li area in EC/DEC and DOL/DME. (f and g) TEM images and (h and i) the histogram for Li particle size after 15 min at 0.5 mA/cm^2 in (f and h) EC/DEC and (g and i) DOL/DME. The scale of *x*-axis in the histograms and the scale bar in the TEM images are different.

electrochemical reaction in the microcell (Figure 1b).[30,31] The galvanostatic method (current density 0.5 mA/cm^2) was employed for electrodeposition of Li. It simulates an actual charging process in the battery system and eliminates current density dependency.[32−34] Upon applying a cathodic current to the working electrode (WE), the voltage instantly reached a nucleation overpotential of −4.1 V (vs Pt pseudoreference), as shown in the voltage profile for galvanostatic plating in EC/DEC (Figure 1c). TEM images were acquired after every 30 s with electron beam blanking between consecutive frames to minimize unwanted beam effects on the electrolyte (Figures 1d and S1). Before the first 3 min, there was no noticeable change in the Pt electrode in the field of view, except for a slightly darkening contrast in the electrode region, indicating the formation of an SEI covering the electrode owing to continuous electroreduction of the electrolyte. Following the first nucleation observed at 3 min (Figure 1d-iii), the formation of new nuclei continued along the electrode surface and covered the entire electrode surface at 10.5 min, as indicated by the red arrows in Figure 1d. In parallel with the continuous nucleation of Li, preformed Li electrodeposits grew into slightly faceted shapes. Notably, nucleation occurred randomly on the surface of the electrode, even though the electrode surface was not flat and had noticeable flaws (marked with blue arrows). This implies that surface defects have no priority for Li nucleation and that there is another important factor for the nucleation of Li, which will be discussed later.

The galvanostatic voltage profile and TEM images of Li plating in DOL/DME are presented in Figures 1e,f and S2, respectively. Despite the same current density applied, the overpotential for Li nucleation, which was −3.2 V (vs Pt pseudoreference), was lower than that in EC/DEC electrolyte. The first nucleation of Li was observed at 4 min, which was slightly later than that in EC/DEC. There were noticeable differences in the Li plating, in contrast to EC/DEC. The size of Li, when it was first observed, was much larger than that in EC/DEC. Additional nucleation events were sparse, and only one nucleation event was observed in the field of view of the TEM snapshots (Figure 1f), in contrast to the continuous and dense Li nucleation observed in EC/DEC. Instead of abundant nucleation, the Li particle formed in DOL/DME rapidly expanded at 7 min and another Li particle suddenly entered the field of view at 8.5 min (labeled as rapid growth 1 and 2, respectively, in Figure 1f-iv,v). Owing to the low overpotential in DOL/DME, the Pt electrode underwent an Li−Pt alloying reaction[33,34] along with Li metal electrodeposition on the surface of the electrode. The Li−Pt alloying on the electrode was confirmed by a roughened electrode surface, volume expansion, and contrast change of the electrode, as shown in Figures 1f and S3. After Li−Pt alloying, Li was electrodeposited as an island

https://doi.org/10.1021/acsenergylett.2c02387
ACS Energy Lett. 2023, 8, 715−721

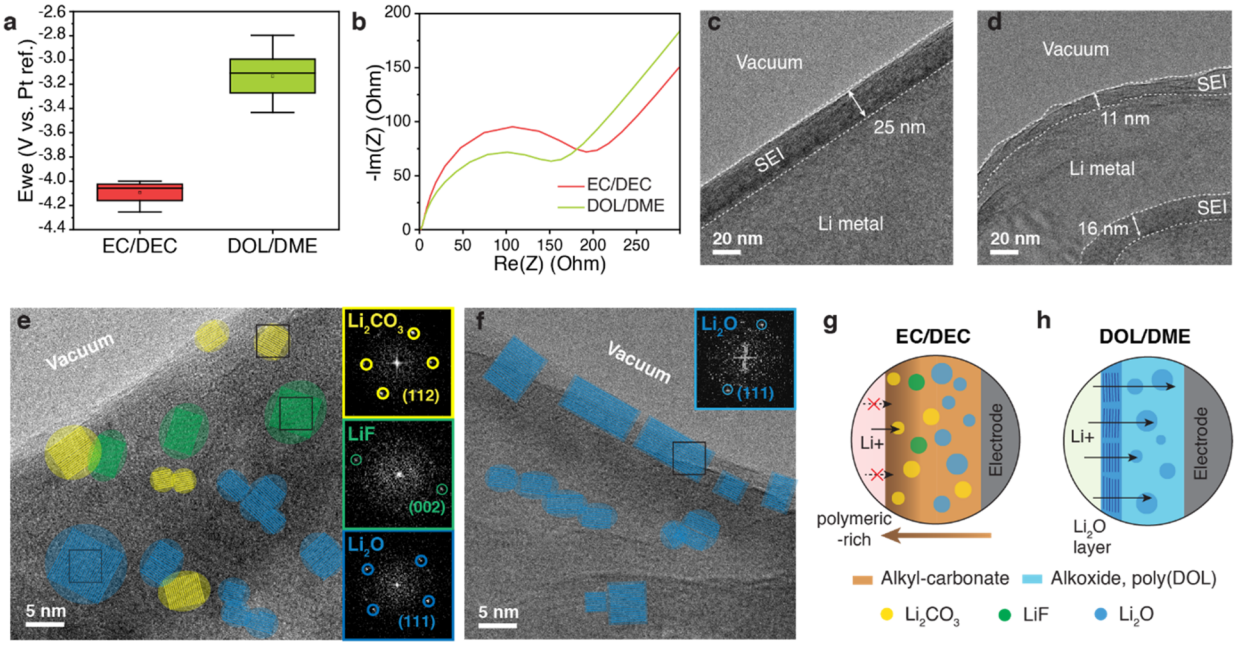

Figure 3. (a) The box plot for nucleation overpotential during galvanostatic experiment at 0.5 mA/cm^2 in EC/DEC and DOL/DME electrolytes. (b) Electrochemical impedance spectroscopy Nyquist plots after SEI formation in EC/DEC and DOL/DME electrolytes. Cryogenic-TEM (Cryo-TEM) images of Li metal and SEI layer deposited in (c) EC/DEC and (d) DOL/DME. High-resolution TEM images of SEI region from (e) EC/DEC and (f) DOL/DME. The fast Fourier transform patterns of Li_2CO_3, LiF, and Li_2O are shown in insets. Schemes of SEI structure formed in (g) EC/DEC and (h) DOL/DME.

with an extended interface with the electrode, which is visible along the boundary of the electrode from 11.5 min.

We conducted a quantitative comparison of the *in situ* liquid phase TEM observations from the two electrolyte systems. A number of nuclei were gradually generated in EC/DEC, whereas only a single event of nucleation was observed in DOL/DME, within the uniform field of view (except the particle nucleated outside the field of view), as shown in Figure 2a. The average size of the Li particles on their first appearance in EC/DEC, measured from 19 Li nuclei, was 0.015 μm^2, which was much smaller than that (0.078 μm^2) in DOL/DME. The growth rate of the individual particles in DOL/DME was larger, approximately 15−40 times higher than that in EC/DEC (Figure 2b). The trend in change in growth rate was also different. Li particles in EC/DEC grew linearly at a slow growth rate (Figure S4). In contrast, the particles in DOL/DME grew in a unique way. The size of Li increased explosively after a short period when the growth was seemingly paused and then approached a retarded growth stage, as confirmed by the particle contours during growth (Figure 2c). The rapid expansion in DOL/DME can explain the sudden appearance of additional Li particles in the field of view at 8.5 min (Figure 1f). An interesting difference was also found in the total projected area of all Li particles within the frame (Figure 2d). The areas in the two electrolytes were comparable up to 8 min, after which the area in DOL/DME greatly exceeded that in EC/DEC, and the gap further widened, as clearly shown in the plot of the area difference (Figure 2e). This indicates that the amount of Li electrodeposited in DOL/DME was greater than that in EC/DEC. Considering the additional consumption of Li in the alloying reaction, the difference in the amount of electrodeposited Li was much larger. This further implies that there are severe irreversible side reactions, such as electrolyte decomposition during the initial Li formation process in EC/DEC. This result is in accordance with the well-known low Coulombic efficiency problem in LMBs operated with EC/DEC electrolyte due to the high reactivity of carbonate-based solvents with Li.[4,27,35] Further difference between two electrolytes is also found in the coverage of the electrode tracked with capacity, as discussed in Supplementary Note 1 (Figure S5). The size of Li particles after 15 min (at 0.125 mA h/cm^2) in the two electrolytes was measured. Whereas the average size in EC/DEC was 0.15 μm^2 (Figure 2f,h), in DOL/DME it was 2.71 μm^2, approximately 18.1 times larger, with a broader size distribution (Figure 2g,i). Owing to the large volume of Li formed in DOL/DME, the adjacent Li particles can be deformed. Moreover, secondary particles nucleated on the primary particles, which was presumably attributed to the cracking of the SEI.

As already mentioned, the nucleation overpotential differs depending on the electrolyte, which may affect the initial electrodeposition pattern of Li. This was validated by multiple experiments demonstrating that the nucleation overpotential in EC/DEC was significantly larger than that in DOL/DME (Figure 3a). The nucleation overpotential (Figure S6) in the coin cell (Li|Cu half-cell) also confirmed a similar tendency. The overpotential difference measured in the liquid microcell and coin cell was possibly due to the distinct geometry of the liquid microcell (Supplementary Notes 2 and 3 and Figure S7). This large overpotential gap is mainly attributed to the different kinetic properties of the SEI. We evaluated the kinetic properties of the SEIs in the two electrolytes using electrochemical impedance spectroscopy (Figure 3b). The results showed that the resistance to Li-ion transport through the SEI in EC/DEC (192 Ω) was larger than that in DOL/DME (151 Ω), which accounted for the high overpotential in EC/DEC. To investigate the SEI structures uniformly formed in each electrolyte at the same current density as in the liquid phase TEM experiment, we performed cryo-TEM and electron energy loss spectroscopy (EELS) analyses. A thick SEI layer of 20−30 nm was observed in EC/DEC, confirmed by the apparent dark contrast on the

https://doi.org/10.1021/acsenergylett.2c02387
ACS Energy Lett. 2023, 8, 715−721

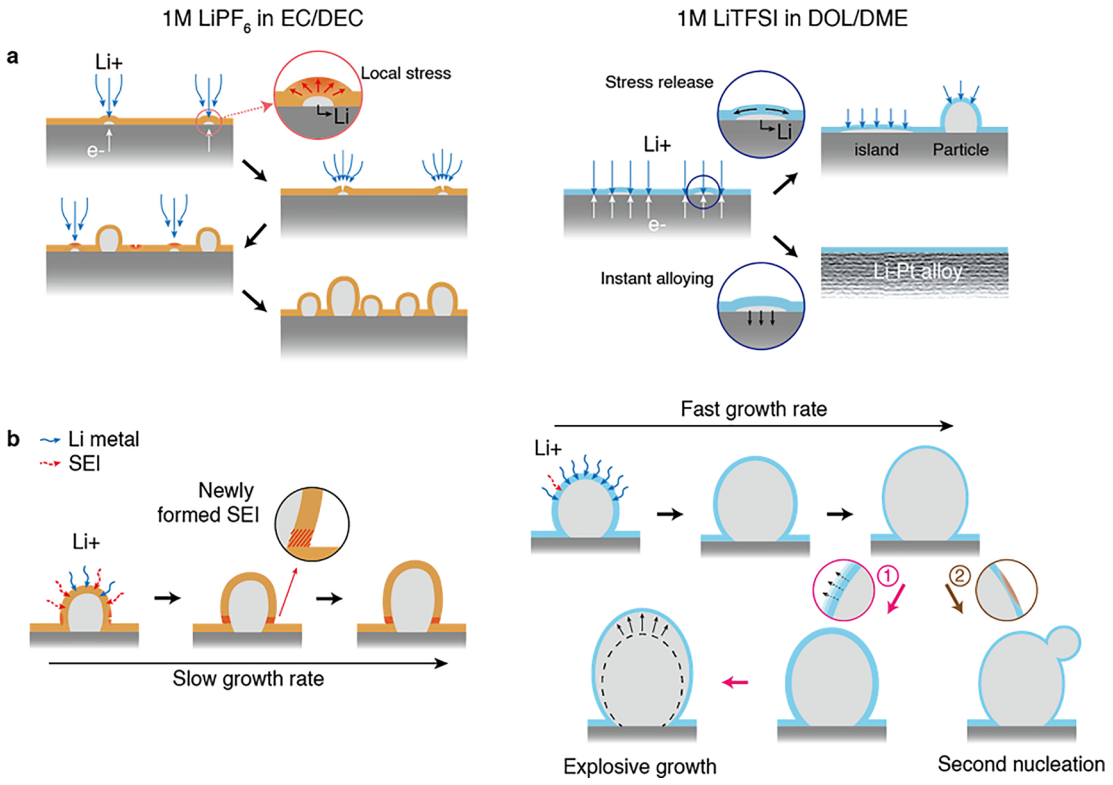

Figure 4. Schematic illustrations of the mechanisms of (a) Li nucleation and (b) growth during the early stage of Li plating in EC/DEC and DOL/DME.

surface of the Li metal (Figure 3c) and the Li K-edge in EELS (Figure S8a). The high-resolution TEM (HR-TEM) image and fast Fourier transform (FFT) patterns of the SEI in EC/DEC (Figure 3e) show that multiple ionic species including Li_2CO_3, LiF, and Li_2O were heterogeneously distributed in the amorphous organic matrix. The EELS line scan for SEI (Figure S8b) shows that carbon is mainly present in the outer layer, while oxygen has the highest proportion in the inner layer above the Li metal, which corresponds to the bright contrast area of the high-angle annular dark field scanning transmission electron microscopy (HAADF-STEM) image. However, a thin SEI layer of 10−20 nm was formed in DOL/DME, as confirmed by the contrast (Figure 3d) in the TEM image and Li K-edge in EELS (Figure S8c). The HR-TEM image and FFT pattern indicate that multilayered Li_2O covered the outer region of the SEI, where it interfaced with the electrolyte (Figure 3f). Moreover, beneath the multilayered Li_2O, there was an amorphous organic matrix in which Li_2O crystalline grains were distributed. The EELS line scan for the SEI in DOL/DME indicated that oxygen and carbon had similar trends in distribution throughout the SEI (Figure S8d), implying that there was no distinct localization of organic-rich and inorganic-rich regions in the SEI. Based on these results, we clarified the SEI structure in EC/DEC and DOL/DME, as illustrated in Figure 3g,h. For EC/DEC, the SEI was formed as a double layer. The outer layer close to the electrolyte had an organic-rich matrix in which the Li_2CO_3 and LiF crystalline phases were irregularly positioned. The inner layer near the Li metal contained more inorganic components with Li_2O and Li_2CO_3 crystalline phases. The ionic species that are randomly distributed with nanoscale domains within the organic-rich surface limit the continuous path for Li diffusion, inducing nonuniform and slow Li^+ transport. In DOL/DME, the outermost layer uniformly consisted of dense multilayered Li_2O grains, thereby improving the Li-ion conductivity, and the inner layer was composed of an amorphous organic matrix with embedded Li_2O nanocrystallites. Owing to the difference in SEI structures, each SEI has disparate resistance, which causes an overpotential gap that affects the Li nucleation and growth behavior. In addition, as EC/DEC is vulnerable to electrolyte decomposition owing to its high reactivity with Li metal and the low cathodic stability of carbonate-based solvents,[27,35,36] kinetic competition between the electrodeposition of pure Li metal and side reactions of electrolytes increases the overpotential in EC/DEC.

Based on the *in situ* and cryo-TEM observations of the early stage Li plating and SEI structures, the mechanisms for Li nucleation in EC/DEC and DOL/DME are shown in Figure 4a. Upon applying current to the cell, the SEI film was instantly deposited on the WE prior to Li nucleation. In EC/DEC, uneven Li^+ flux through the inhomogeneous SEI lead to the accumulation of Li atoms at specific sites under the SEI, causing local stress on the SEI. The stressed SEI is likely to be broken owing to its fragility.[4,26] The crack formed on the SEI and locally exposed electrode surface further promotes the concentration of Li^+ flux, by which the nucleation of Li particles appears outside the predeposited SEI film. It was also observed that Li nucleation did not preferentially occur at the electrode defect sites, indicating that the inhomogeneity of the SEI determined the spots where Li nucleation events occur (Figure 1d). As the nucleation process induces stress on the surrounding SEI, a series of nucleation events can occur through the brittle SEI over the electrode, resulting in continuous and dense nucleation. However, in the case of DOL/DME, the SEI covered by uniform multilayered Li_2O grains with high ionic conductivity facilitated relatively homogeneous and fast Li reduction under the SEI. As the SEI matrix includes flexible alkoxide and poly DOL,[4,37,38]

https://doi.org/10.1021/acsenergylett.2c02387
ACS Energy Lett. 2023, 8, 715−721

crack formation on the SEI is likely rare, leading to sparse nucleation of Li particles. Moreover, the reduced Li with a large interface area can grow to form a Li island or instantly react with Pt to form a Li−Pt alloy.

The mechanisms for the growth of single Li particles in the two electrolytes are presented in Figure 4b. In EC/DEC, limited Li^+ penetration through the double-layered SEI caused individual Li particles to grow slowly. During the expansion of the Li particles, cracks continually form on the SEI because of the fragile nature, and the surface of the Li metal was exposed, which was immediately passivated with the extended formation of a new SEI. In addition, the high reactivity of organic components and Li_2CO_3 at the outer layer[21] prompted the consumption of incoming Li^+ by a side reaction with the electrolyte, which slowed down the growth of Li particles. In DOL/DME, owing to the facile transportation of Li^+ through the SEI, the Li particles grew faster than those in EC/DEC. The flexibility of the SEI also contributed to the fast growth of Li particles by accommodating a large amount of Li reduction. Meanwhile, we observed a unique growth process, including retarded and explosive growth regimes in DOL/DME, which was different from the gradual growth in EC/DEC. As the Li particles grow, the flexible SEI stretches and becomes thin. The thinned SEI allows electrons to penetrate and reduce ionic conductivity. Upon reaching the elastic limit of the SEI, the growth of Li can be paused. The growth rate of Li can increase after the formation of a stable SEI during this retardation stage. Alternatively, cracks can form on the SEI at its elastic limit, leading to secondary nucleation over a primary Li particle.

To summarize, the initial Li electrodeposition process in the two electrolytes was investigated using *in situ* liquid phase TEM and cryo-TEM analysis. We revealed that the nucleation and early growth of each Li particle were determined by the chemical structure and mechanical properties of the SEI from each electrolyte. While slow and gradual Li growth with high nucleation density is induced in EC/DEC due to low Li^+ diffusivity and poor stability of the SEI, Li grows rapidly with infrequent nucleation in DOL/DME, owing to the high Li^+ conductivity and flexibility of the SEI. Based on these results, we proposed the mechanism of early stage Li deposition in the two representative electrolytes, highlighting the pivotal role of the SEI in regulating the Li plating dynamics from the very early stage. This study provides important insights for controlling the Li morphology in LMBs by enriching the fundamental understanding of initial growth and can be expanded to further study of the following stage, which can bridge the initial growth and final morphology of Li.

■ ASSOCIATED CONTENT

Supporting Information

The Supporting Information is available free of charge at https://pubs.acs.org/doi/10.1021/acsenergylett.2c02387.

Experimental method, supplementary notes, TEM snapshots during Li plating, TEM image analysis for comparison of Li−Pt alloying, contours of Li particles, coverage with respect to the capacity, Li plating voltage profiles in coin cell, oxidation reaction on counter electrode in microcell, and EELS spectrum (PDF)

Supplementary Movie S1: *In situ* snapshot movie during Li plating in EC/DEC (MP4)

Supplementary Movie S2: *In situ* snapshot movie during Li plating in DOL/DME (MP4)

■ AUTHOR INFORMATION

Corresponding Author

Jungwon Park − *Center for Nanoparticle Research, Institute for Basic Science (IBS) and School of Chemical and Biological Engineering, and Institute of Chemical Process, Seoul National University, Seoul 08826, Republic of Korea; Institute of Engineering Research, College of Engineering, Seoul National University, Seoul 151-742, Republic of Korea; Advanced Institutes of Convergence Technology, Seoul National University, Gyeonggi-do 16229, Republic of Korea;* orcid.org/0000-0003-2927-4331; Email: jungwonpark@snu.ac.kr

Authors

Hayoung Park − *Center for Nanoparticle Research, Institute for Basic Science (IBS) and School of Chemical and Biological Engineering, and Institute of Chemical Process, Seoul National University, Seoul 08826, Republic of Korea;* orcid.org/0000-0002-5926-9165

Yonggoon Jeon − *Center for Nanoparticle Research, Institute for Basic Science (IBS) and School of Chemical and Biological Engineering, and Institute of Chemical Process, Seoul National University, Seoul 08826, Republic of Korea;* orcid.org/0000-0001-5664-1390

Woo Jun Chung − *Center for Nanoparticle Research, Institute for Basic Science (IBS) and School of Chemical and Biological Engineering, and Institute of Chemical Process, Seoul National University, Seoul 08826, Republic of Korea*

Yuna Bae − *Center for Nanoparticle Research, Institute for Basic Science (IBS) and School of Chemical and Biological Engineering, and Institute of Chemical Process, Seoul National University, Seoul 08826, Republic of Korea;* Present Address: Physical Sciences Division, Pacific Northwest National Laboratory, 902 Battelle Boulevard, Richland, Washington 99352, United States

Jihoon Kim − *Center for Nanoparticle Research, Institute for Basic Science (IBS) and School of Chemical and Biological Engineering, and Institute of Chemical Process, Seoul National University, Seoul 08826, Republic of Korea;* orcid.org/0000-0003-2760-2610

Hayeon Baek − *Center for Nanoparticle Research, Institute for Basic Science (IBS) and School of Chemical and Biological Engineering, and Institute of Chemical Process, Seoul National University, Seoul 08826, Republic of Korea*

Complete contact information is available at: https://pubs.acs.org/10.1021/acsenergylett.2c02387

Author Contributions

[▽]H.P. and Y.J. contributed equally.

Notes

The authors declare no competing financial interest.

■ ACKNOWLEDGMENTS

This work was supported by a National Research Foundation of Korea (NRF) grant funded by the Korea government Ministry of Education and Science Technology (MEST) (NRF-2021M3H4A1A02045962). Additionally, this work was also supported by the Hyundai Motor Company.

REFERENCES

(1) Xu, W.; Wang, J.; Ding, F.; Chen, X.; Nasybulin, E.; Zhang, Y.; Zhang, J.-G. Lithium metal anodes for rechargeable batteries. *Energy Environ. Sci.* **2014**, *7*, 513−537.

(2) Cheng, X.-B.; Zhang, R.; Zhao, C.-Z.; Zhang, Q. Toward Safe Lithium Metal Anode in Rechargeable Batteries: A Review. *Chem. Rev.* **2017**, *117*, 10403−10473.

(3) Albertus, P.; Babinec, S.; Litzelman, S.; Newman, A. Status and challenges in enabling the lithium metal electrode for high-energy and low-cost rechargeable batteries. *Nature Energy* **2018**, *3*, 16−21.

(4) Luo, Z.; Qiu, X.; Liu, C.; Li, S.; Wang, C.; Zou, G.; Hou, H.; Ji, X. Interfacial challenges towards stable Li metal anode. *Nano Energy* **2021**, *79*, 105507.

(5) Frenck, L.; Sethi, G. K.; Maslyn, J. A.; Balsara, N. P. Factors That Control the Formation of Dendrites and Other Morphologies on Lithium Metal Anodes. *Front. Energy Res.* **2019**, *7*, 115.

(6) Shi, F.; Pei, A.; Vailionis, A.; Xie, J.; Liu, B.; Zhao, J.; Gong, Y.; Cui, Y. Strong texturing of lithium metal in batteries. *Proc. Natl. Acad. Sci. U. S. A.* **2017**, *114*, 12138−12143.

(7) Kim, H.; Jeong, G.; Kim, Y.-U.; Kim, J.-H.; Park, C.-M.; Sohn, H.-J. Metallic Anodes for next Generation Secondary Batteries. *Chem. Soc. Rev.* **2013**, *42*, 9011−9034.

(8) Lin, D.; Liu, Y.; Cui, Y. Reviving the lithium metal anode for high-energy batteries. *Nat. Nanotechnol.* **2017**, *12*, 194−206.

(9) Qin, N.; Jin, L.; Lu, Y.; Wu, Q.; Zheng, J.; Zhang, C.; Chen, Z.; Zheng, J. P. Over-Potential Tailored Thin and Dense Lithium Carbonate Growth in Solid Electrolyte Interphase for Advanced Lithium Ion Batteries. *Adv. Energy Mater.* **2022**, *12*, 2103402.

(10) Tikekar, M. D.; Choudhury, S.; Tu, Z.; Archer, L. A. Design principles for electrolytes and interfaces for stable lithium-metal batteries. *Nature Energy* **2016**, *1*, 16114.

(11) Chen, H.; Pei, A.; Lin, D.; Xie, J.; Yang, A.; Xu, J.; Lin, K.; Wang, J.; Wang, H.; Shi, F.; Boyle, D.; Cui, Y. Uniform High Ionic Conducting Lithium Sulfide Protection Layer for Stable Lithium Metal Anode. *Adv. Energy Mater.* **2019**, *9*, 1900858.

(12) Shen, X.; Zhang, R.; Chen, X.; Cheng, X.-B.; Li, X.; Zhang, Q. The Failure of Solid Electrolyte Interphase on Li Metal Anode: Structural Uniformity or Mechanical Strength? *Adv. Energy Mater.* **2020**, *10*, 1903645.

(13) Biswal, P.; Stalin, S.; Kludze, A.; Choudhury, S.; Archer, L. A. Nucleation and early stage growth of Li electrodeposition. *Nano Lett.* **2019**, *19*, 8191−8200.

(14) Chen, X.-R.; Yao, Y.-X.; Yan, C.; Zhang, R.; Cheng, X.-B.; Zhang, Q. A Diffusion−Reaction Competition Mechanism to Tailor Lithium Deposition for Lithium-Metal Batteries. *Angew. Chem., Int. Ed.* **2020**, *59*, 7743−7747.

(15) Lee, S. H.; Hwang, J.-Y.; Ming, J.; Kim, H.; Jung, H.-G.; Sun, Y.-K. Long-Lasting Solid Electrolyte Interphase for Stable Li-Metal Batteries. *ACS Energy Lett.* **2021**, *6*, 2153−2161.

(16) Younesi, R.; Veith, G. M.; Johansson, P.; Edström, K.; Vegge, T. Lithium salts for advanced lithium batteries: Li−metal, Li−O_2, and Li−S. *Energy Environ. Sci.* **2015**, *8*, 1905−1922.

(17) Wu, H.; Jia, H.; Wang, C.; Zhang, J.-G.; Xu, W. Recent Progress in Understanding Solid Electrolyte Interphase on Lithium Metal Anodes. *Adv. Energy Mater.* **2021**, *11*, 2003092.

(18) Huang, W.; Wang, H.; Boyle, D. T.; Li, Y.; Cui, Y. Resolving Nanoscopic and Mesoscopic Heterogeneity of Fluorinated Species in Battery Solid-Electrolyte Interphases by Cryogenic Electron Microscopy. *ACS Energy Lett.* **2020**, *5*, 1128−1135.

(19) Nanda, J.; Yang, G.; Hou, T.; Voylov, D. N.; Li, X.; Ruther, R. E.; Naguib, M.; Persson, K.; Veith, G. M.; Sokolov, A. P. Unraveling the Nanoscale Heterogeneity of Solid Electrolyte Interphase Using Tip-Enhanced Raman Spectroscopy. *Joule* **2019**, *3*, 2001−2019.

(20) Piao, N.; Liu, S.; Zhang, B.; Ji, X.; Fan, X.; Wang, L.; Wang, P.-F.; Jin, T.; Liou, S.-C.; Yang, H.; Jiang, J.; Xu, K.; Schroeder, M. A.; He, X.; Wang, C. Lithium Metal Batteries Enabled by Synergetic Additives in Commercial Carbonate Electrolytes. *ACS Energy Lett.* **2021**, *6*, 1839−1848.

(21) Han, B.; Zhang, Z.; Zou, Y.; Xu, K.; Xu, G.; Wang, H.; Meng, H.; Deng, Y.; Li, J.; Gu, M. Poor Stability of Li_2CO_3 in the Solid Electrolyte Interphase of a Lithium-Metal Anode Revealed by Cryo-Electron Microscopy. *Adv. Mater.* **2021**, *33*, 2100404.

(22) Jiao, S.; Ren, X.; Cao, R.; Engelhard, M. H.; Liu, Y.; Hu, D.; Mei, D.; Zheng, J.; Zhao, W.; Li, Q.; Liu, N.; Adams, B. D.; Ma, C.; Liu, J.; Zhang, J.-G.; Xu, W. Stable cycling of high-voltage lithium metal batteries in ether electrolytes. *Nature Energy* **2018**, *3*, 739−746.

(23) Tan, Y.-H.; Lu, G.-X.; Zheng, J.-H.; Zhou, F.; Chen, M.; Ma, T.; Lu, L.-L.; Song, Y.-H.; Guan, Y.; Wang, J.; Liang, Z.; Xu, W.-S.; Zhang, Y.; Tao, X.; Yao, H.-B. Lithium Fluoride in Electrolyte for Stable and Safe Lithium-Metal Batteries. *Adv. Mater.* **2021**, *33*, 2102134.

(24) Pei, A.; Zheng, G.; Shi, F.; Li, Y.; Cui, Y. Nanoscale Nucleation and Growth of Electrodeposited Lithium Metal. *Nano Lett.* **2017**, *17*, 1132−1139.

(25) Xu, X.; Jiao, X.; Kapitanova, O. O.; Wang, J.; Volkov, V. S.; Liu, Y.; Xiong, S. Diffusion Limited Current Density: A Watershed in Electrodeposition of Lithium Metal Anode. *Adv. Energy Mater.* **2022**, *12*, 2200244.

(26) Sung, J.; Bae, Y.; Park, H.; Kang, S.; Choi, B. K.; Kim, J.; Park, J. Liquid-Phase Transmission Electron Microscopy for Reliable In Situ Imaging of Nanomaterials. *Annu. Rev. Chem. Biomol. Eng.* **2022**, *13*, 167−191.

(27) Pu, J.; Zhong, C.; Liu, J.; Wang, Z.; Chao, D. Advanced *in situ* technology for Li/Na metal anodes: as in-depth mechanistic understanding. *Energy Environ. Sci.* **2021**, *14*, 3872−3911.

(28) Li, Y.; Li, Y.; Pei, A.; Yan, K.; Sun, Y.; Wu, C.-L.; Joubert, L.-M.; Chin, R.; Koh, A. L.; Yu, Y.; Perrino, J.; Butz, B.; Chu, S.; Cui, Y. Atomic structure of sensitive battery materials and interfaces revealed by cryo−electron microscopy. *Science* **2017**, *358*, 506−510.

(29) Ren, X.-C.; Zhang, X.-Q.; Xu, R.; Huang, J.-Q.; Zhang, Q. Analyzing Energy Materials by Cryogenic Electron Microscopy. *Adv. Mater.* **2020**, *32*, 1908293.

(30) Kuwata, N.; Iwagami, N.; Matsuda, Y.; Tanji, Y.; Kawamura, J. Thin Film Batteries with Li3PO4 Solid Electrolyte Fabricated by Pulsed Laser Deposition. *ECS Trans.* **2009**, *16*, 53.

(31) Park, S. H.; Winnick, J.; Kohl, A. A. Investigation of the Lithium Couple on Pt, Al, and Hg Electrodes in Lithium Imide-Ethyl Methyl Sulfone. *J. Electrochem. Soc.* **2002**, *149*, A1196−A1200.

(32) Dong, K.; Xu, Y.; Tan, J.; Osenberg, M.; Sun, F.; Kochovski, Z.; Pham, D. T.; Mei, S.; Hilger, A.; Ryan, E.; Lu, Y.; Banhart, J.; Manke, I. Unravelling the Mechanism of Lithium Nucleation and Growth and the Interaction with the Solid Electrolyte Interface. *ACS Energy Lett.* **2021**, *6*, 1719−1728.

(33) Yan, K.; Lu, Z.; Lee, H.-W.; Xiong, F.; Hsu, P.-C.; Li, Y.; Zhao, J.; Chu, S.; Cui, Y. Selective deposition and stable encapsulation of lithium through heterogeneous seeded growth. *Nature Energy* **2016**, *1*, 16010.

(34) Kushima, A.; So, K. P.; Su, C.; Bai, P.; Kuriyama, N.; Maebashi, T.; Fujiwara, Y.; Bazant, M. Z.; Li, J. Liquid cell transmission electron microscopy observation of lithium metal growth and dissolution: Root growth, dead lithium and lithium flotsams. *Nano Energy* **2017**, *32*, 271−279.

(35) Yang, C.; Fu, K.; Zhang, Y.; Hitz, E.; Hu, L. Protected Lithium-Metal Anodes in Batteries: From Liquid to Solid. *Adv. Mater.* **2017**, *29*, 1701169.

(36) Yaakov, D.; Gofer, Y.; Aurbach, D.; Halalay, I. C. On the Study of Electrolyte Solutions for Li-Ion Batteries That Can Work Over a Wide Temperature Range. *J. Electrochem. Soc.* **2010**, *157*, A1383−A1391.

(37) Aurbach, D. Review of selected electrode-solution interactions which determine the performance of Li and Li ion batteries. *J. Power Sources* **2000**, *89*, 206−218.

(38) Zhao, Q.; Liu, X.; Stalin, S.; Khan, K.; Archer, L. A. Solid-state polymer electrolytes with in-built fast interfacial transport for secondary lithium batteries. *Nature Energy* **2019**, *4*, 365−373.

https://doi.org/10.1021/acsenergylett.2c02387
ACS Energy Lett. 2023, 8, 715−721